Enhanced Linear Active Disturbance Rejection Speed Control of IPMSM Based on Interference Differential Compensation and Cascaded Linear Extended State Observer

Yangyang Cui, Zhonggang Yin, *Member, IEEE*, Xiaobo Cao, Yanqing Zhang, *Member, IEEE*, and Yiqi Liu, *Member, IEEE*

***Abstract*—Due to the influence of bandwidth, the interior permanent magnet synchronous motor (IPMSM) control system based on a traditional linear active disturbance rejection controller has a coupling issue between tracking and interference compensation capability. To deal with the above issue, an enhanced linear active disturbance rejection controller (E-LADRC) combining interference differential compensation and cascaded linear extended state observer (IDC-C-LESO) is proposed in this article. Based on the traditional LESO, the lumped interference differential signal is introduced into the E-LADRC so that the scope observation of the lumped interference is widened by LESO, and the system instability caused by the oversized bandwidth of the observer is avoided. C-LESO is used to reduce the observation error of LESO to the lumped interference. The IPMSM outer loop controller based on E-LADRC is established in this article, and its control characteristic is analyzed. Finally, the control characteristic of E-LADRC is verified through experiment.**

***Index Terms*—Active disturbance rejection control, extended state observer (ESO), permanent magnet synchronous motor (PMSM), robust control, stability.**

NOMENCLATURE

ω_r, ω_r^*, $\hat{\omega}_r$	Actual value, given value, and observed value of mechanical angular velocity, rad/s.
T_e, T_L	Electromagnetic torque and load torque, N·m.
B_r	Damping coefficient.
d_r	External interference.
ΔJ, $\bar{J}$, J, $\hat{J}$	Change in value, nominal value, actual value, and observed value of moment of inertia, kg·m^2.
x_1, x_2	State variables of system output and unknown interference.
z_1, z_2, z_3	Observed values of state variables for system output, lumped interference, and lumped interference differential.
β_1, β_2, β_3	Error feedback gain coefficients of IDC-LESO1.
l_1, l_2, l_3	Error feedback gain coefficients of IDC-LESO2.
b_0	Compensation factor.
k_p	Control gain of LSEF.
r	Reference signal for LADRC.
u_0, u	Output of LSEF and LADRC.
ω_c, ω_o	The LSEF and LESO bandwidth of LADRC, rad/s.
f, $\hat{f}$, $\dot{f}$	Actual value, observed value, and differential of lumped interference for IDC-LESO1.
γ,$\hat{\gamma}$,$\dot{\gamma}$	Actual value, observed value, and differential of lumped interference for IDC-LESO2.
PMSM	Permanent magnet synchronous motor.
SPMSM	Surface-mounted permanent magnet synchronous motor.
IPMSM	Interior permanent magnet synchronous motor.
MTPA	Maximum torque per ampere.
FOC	Field-oriented control.
PI	Proportional integral.
ADRC	Active disturbance rejection controller.
NLADRC	Nonlinear active disturbance rejection controller.
LADRC	Linear active disturbance rejection controller.
LESO	Linear extended state observer.
LSEF	Linear state error feedback.
LTD	Linear tracking differentiator.
T-LADRC	Traditional linear active disturbance rejection controller.
E-LADRC	Enhanced linear active disturbance rejection controller.

Manuscript received 27 April 2024; accepted 22 June 2024. Date of publication 26 June 2024; date of current version 4 September 2024. This work was supported in part by the National Natural Science Foundation of China under Grant 52177194 and Grant 52107206, in part by the China Postdoctoral Science Foundation under Grant 2020M683524, in part by the Natural Science Basic Research Plan in Shaanxi Province under Grant 2022GY-016 and Grant 2022JQ-538, and in part by the Science and Technology Innovation Team in Shaanxi Province under Grant 2023-CX-TD-23. Recommended for publication by Associate Editor L. Iyer. *(Corresponding author: Zhonggang Yin.)*

Yangyang Cui, Zhonggang Yin, Xiaobo Cao, and Yanqing Zhang are with the Department of Electrical Engineering, Xi'an University of Technology, Xi'an 710054, China (e-mail: 1211913014@stu.xaut.edu.cn; zhgyin@xaut.edu.cn; 1231910007@stu.xaut.edu.cn; zhangyanqing@xaut.edu.cn).

Yiqi Liu is with the College of Mechanical and Electrical Engineering, Northeast Forestry University, Harbin 150040, China (e-mail: ee_617@nefu.edu.cn).

Color versions of one or more figures in this article are available at https://doi.org/10.1109/TPEL.2024.3419247.

Digital Object Identifier 10.1109/TPEL.2024.3419247

IDC-LADRC	Linear active disturbance rejection controller based on interference differential compensated linear extended state observer.
C-LADRC	Linear active disturbance rejection controller based on cascaded linear extended state observer.
T-LESO	Traditional linear extended state observer.
C-LESO	Cascaded linear extended state observer.
IDC-LESO	Interference differential compensation linear extended state observer.
IDC-C-LESO	Interference differential compensation and cascaded linear extended state observer.

I. Introduction

COMPARED with alternating current asynchronous motors, the PMSM has superiorities, such as dynamic characteristics and energy conservation [1]. Its application fields have expanded from electrical automation fields, such as substations and petroleum smelting, to military fields, such as radar monitoring and weapon equipment [2]. Compared to SPMSM, the reluctance torque of IPMSM can be fully utilized by IPMSM to further improve its load-bearing capacity, which has attracted widespread attention. At present, the FOC based on MTPA control is used by the IPMSM control system [3]. Among them, the outer loop controller is taken as the reference signal of the inner loop controller in the FOC system and has a pivotal position. In the various characteristic indicators of IPMSM control systems, tracking and interference compensation capability are considered the focus and difficulty of research in the field of IPMSM control systems. The main reason is the diversity of interference sources, rich frequency spectrum, and random timing. The outer loop of the IPMSM control system is usually influenced by both parameter mismatch and load interference. Therefore, the mechanism and characteristics of interference generation will be analyzed, and the theoretical and application system of IPMSM interference suppression technology will be improved, which is particularly urgent.

In response to the aforementioned interference types, the traditional PI controller is held in an important position in the IPMSM control system [4]. However, when the system is affected by lumped interference, it is difficult for a traditional PI controller to effectively control it. According to this issue, two degrees of freedom PI control [5], sliding mode variable structure control [6], backstepping control [7], dynamic fuzzy neural network control [8], extended Kalman filter control [9], robust adaptive model predictive control [10], and fuzzy adaptive ADRC [11], [12] are adopted in the motor control system. Among them, the concept of "model theory" in the traditional control theory is abandoned by ADRC, and "engineering cybernetics" is taken as the core. The parts of the system that are different from the standard type are attributed to the lumped interference. The lumped interference is observed and compensated in real time through ADRC [13]. However, nonlinear functions are mostly used by NLADRC, which are complex in structure and numerous in parameters. This has to some extent affected the promotion and application of ADRC. Its stability boundary is difficult to determine by the commonly used frequency domain analysis method. To deal with the issue of parameter setting and theoretical analysis, the LADRC is proposed by Gao [14]. The controller parameters of LADRC are correlated with bandwidth frequency, thus clarifying the actual engineering meaning of ADRC parameters. Meanwhile, compared with NLADRC, the stability domain of LADRC can be determined by frequency domain analysis methods. However, the development of NLADRC to LADRC is only for the purpose of better simplifying its application and promoting it to the industrial field and does not necessarily mean that the control characteristic of LADRC is superior to that of NLADRC. At present, large time delay systems cannot be effectively regulated by LADRC.

Combining complex interference and different operating conditions, numerous improvement methods for LADRC have been proposed by many researchers and applied to the field of industrial control. In [15], to reveal the relationship between the ten different ADRCs based on the fourth-order generalized PI observer and the ADRC based on the third-order ESO, six different third-order-ESO-based ADRC are present and compared with the fourth-order-LESO-based ADRC. Thus, it can be concluded that interference in different frequency bands can be effectively observed and compensated using corresponding controllers. At the same time, in LSEF, the proportional feedback control is replaced by the PI feedback control, which improves the low-frequency interference suppression ability of the system and has a relatively small impact on other dynamic performance. However, the oversaturation problem caused by the integrator has not been effectively resolved. In [16], an adaptive ADRC suitable for the current loop of IPMSM drive system is proposed, aiming to suppress current ripple caused by periodic and aperiodic interferences. In [17], to improve the control performance of IPMSM sensorless control technology from zero-speed to low-speed operating conditions, a high-frequency voltage pulse injection method based on E-LADRC is proposed. The C-LESO is established in this E-LADRC, ensuring that the lumped interference is observed relatively timely and accurately. In [18], a novel nonlinear active disturbance rejection speed loop controller for PMSM drive system is proposed to expand the observation range of lumped disturbance and improve the robustness of the system. Due to the consideration of the accuracy and dynamic performance of interference observation, traditional linear function is replaced by nonlinear function in this controller. To ensure relatively fast and accurate interference observation and compensation, a cascaded nonlinear ESO is also constructed. In [19], an improved LADRC is proposed. The error proportion feedback term is added to LESO. Meanwhile, a high-pass filter is used as the velocity compensator at the LSEF. As a result, the ability of the PMSM drive system to observe load interference during low-speed operation is greatly enhanced, and speed fluctuations are reduced. The control method proposed above has improved its ability to suppress lumped interference. However, when influenced by the observer bandwidth ω_o, the coupling issue between tracking and interference compensation capability brought by the system under complex interference and different operating conditions still cannot be resolved by

LADRC. The system instability will be caused by oversized ω_o. If ω_o is too small, the lumped interference of the system cannot be accurately observed. T-LESO has tracking errors for rapidly changing interference. At the same time, the problem of difficult parameter setting in the control methods proposed by the aforementioned references (especially in the case of ADRC with nonlinear functions) cannot be reasonably solved.

To deal with the above issues, an E-LADRC is proposed in this article. This controller is introduced with a lumped interference differential signal based on LESO. The IDC-LESO is embedded into the LADRC in a cascade manner. The innovation and contribution of this article can be included as follows.

1) In terms of interference observation compensation and tracking performance, the IDC-C-LESO proposed in this article is compared with the improved LADRC proposed in [15], [17], [20], and [21]. First, a differential signal with lumped interference is introduced into the LESO in E-LADRC. Therefore, under the condition that ω_o is not increased, the observation range of LESO for lumped interference is expanded, and the problem of system oscillation caused by excessive ω_o is avoided. In this way, the high-frequency interference received by the system can be effectively observed and compensated without the need to introduce other control methods, thereby reducing the complexity of the algorithm. Then, the C-LESO based on IDC-LESO (IDC-C-LESO) is adopted so that the high-order interference (such as acceleration interference) experienced by the system can be effectively observed and compensated. Meanwhile, the coupling problem between system traceability and anti-interference can also be solved by IDC-C-LESO.
2) While the system control performance is improved, the controller parameter setting problem is also taken into account by the method proposed in this article. In terms of parameter setting, the controller is closely combined with IPMSM equations of motion, and the compensation factor b_0 is configured with the motor moment of inertia J. Meanwhile, the setting method for ω_o and controller bandwidth ω_c is provided so that the final parameter that needs to be set is only ω_o. Compared with the controllers proposed in [18], [22], and [23], this method not only solves the coupling problem of anti-interference and tracking but also greatly reduces the difficulty of parameter setting.
3) The E-LADRC proposed in this article is a universal controller. This controller can be applied not only to IPMSM drive systems but also to other alternating current/direct current motor control systems, special operating conditions (weak magnetic acceleration [24]) and electric vehicle control systems to demonstrate its optimal control performance (electric vehicles are single loop control systems with only a current inner loop [25], and the current inner loop PI controller can be replaced by E-LADRC to improve the dynamic characteristics of the entire system).

The rest of the article is organized as follows. In Section II, the IPMSM outer loop controller based on T-LADRC is established. In Section III, a detailed introduction is given to the E-LADRC, and an IPMSM outer loop controller based on E-LADRC is presented. In Section IV, the stability, anti-interference and tracking characteristics of the E-LADRC are certificated. At the same time, the setting range of the controller parameters is provided. In Section V, the control characteristic of the E-LADRC is proved by 2-kW experimental platform. The work of the entire article is summarized in the final section, and future work plans are elaborated.

II. Establishment of IPMSM Mathematical Model Based on T-LADRC

The design of the IPMSM speed loop controller mainly depends on the motion equation under rotating coordinates. Therefore, an accurate mathematical model of IPMSM in a rotating coordinate system should be established. At this point, it is assumed that IPMSM is an ideal motor and the following conditions must be met [26].

1) The saturation of the motor core is ignored.
2) The eddy current and hysteresis losses in the motor are ignored.
3) The current in the motor is a symmetrical three-phase sine wave motor.

While satisfying the above assumptions, it is necessary to ensure that the entire system is a three-phase symmetrical system. By coordinate transformation, the IPMSM motion equation with moment of inertia mismatch can be obtained as follows:

$$\begin{cases} \dot{\omega}_r = \frac{1}{\bar{J}} T_e - \frac{1}{\bar{J}} T_L \mp \frac{\Delta J}{\bar{J}} \dot{\omega}_r - \frac{B_r}{\bar{J}} \omega_r + d_r \\ J = \bar{J} \pm \Delta J \end{cases}. \tag{1}$$

From (1), the IPMSM control system will be controlled by the first-order LADRC. Due to the noise signal in the system being amplified by LTD in LADRC, it can cause system oscillation and even instability. Therefore, the LTD is not used in this paper [27]. About first-order controlled object $\dot{y} = f(y,w,t) + b_0 u$, $y = x_1$ and $f = x_2$ are selected as state variables. The T-LADRC is shown as follows:

$$\begin{cases} \left.\begin{aligned} \dot{z}_1 &= z_2 - \beta_1 (z_1 - x_1) + b_0 u \\ \dot{z}_2 &= -\beta_2 (z_1 - x_1) \end{aligned}\right\} \text{LESO} \\ u_0 = k_p (r - z_1) \text{ LSEF} \\ u = \frac{u_0 - z_2}{b_0} \end{cases}. \tag{2}$$

Through pole configuration, β_1 and β_2 are configured at ω_o and k_p is configured at ω_c [28] as

$$\begin{cases} s^2 + \beta_1 s + \beta_2 = (s + \omega_o)^2 \\ s + k_p = s + \omega_c \end{cases}. \tag{3}$$

According to (3), $\beta_1 = 2\omega_o$, $\beta_2 = \omega_o^2$, and $k_p = \omega_c$.

The control structure diagrams of T-LADRC and T-LESO can be obtained from (2) and (3), as shown in Fig. 1.

For T-LADRC, as shown in (2), (3), and Fig. 1, it is mainly composed of three parts: LSEF, LESO, and lumped interference compensation link. Among them, the LSEF is mainly used to control the generation of variables. The main function of LESO is to observe the lumped interference received by the system. The main function of the lumped interference compensation link is

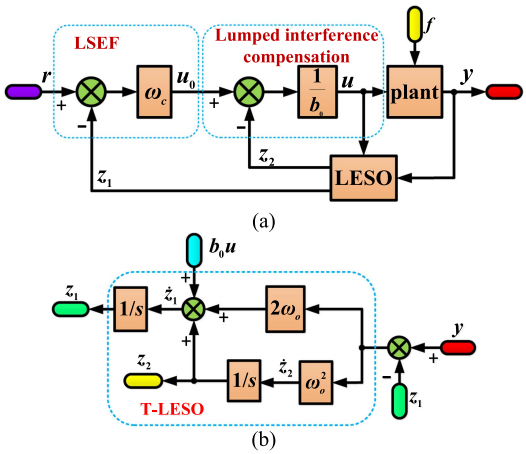

Fig. 1. Control structure diagrams of T-LADRC and T-LESO. (a) T-LADRC. (b) T-LESO.

to combine the effect of LSEF to eliminate the system's lumped interference observed by LESO.

From (1), ω_r is selected as the state variable, and the equation of state of IPMSM is shown in as follows:

$$\begin{cases} \dot{\omega}_r = f + b_0 T_e \\ b_0 = \frac{1}{J} \\ f = \mp\frac{\Delta J}{J}\dot{\omega}_r - \frac{1}{J}T_L - \frac{B_r}{J}\omega_r + d_r \end{cases}. \tag{4}$$

In (4), $\mp\frac{\Delta J}{J}\dot{\omega}_r - \frac{B_r}{J}\omega_r$ is the internal interference of the system, and $-\frac{1}{J}T_L + d_r$ is the external interference of the system. Among them, internal interferences include moment of inertia mismatch and mechanical friction generated by the motor during operation. External interferences mainly include load interference and other external interferences imposed on the system. Due to the uncertainty of each component in the lumped interference, each interference component of the lumped interference *f* will be observed and compensated as an unknown interference.

From (1) to (4), the IPMSM outer loop controller based on T-LADRC is shown as

$$\begin{cases} \dot{\hat{\omega}}_r = \hat{f} - 2\omega_o\left(\hat{\omega}_r - \omega_r\right) + b_0 T_e \\ \dot{\hat{f}} = -\omega_o^2\left(\hat{\omega}_r - \omega_r\right) \\ u_0 = \omega_c\left(\omega_r^* - \hat{\omega}_r\right) \\ T_e = \frac{u_0 - \hat{f}}{b_0} \end{cases}. \tag{5}$$

III. Design of Enhanced Linear Active Disturbance Rejection Controller

A. Interference Differential Compensation Linear Extended State Observer

To broaden the observation scope of the lumped interference by LESO without increasing ω_o, so that the lumped interference can be accurately observed by LESO. The IDC-LESO is established as shown in the following equation:

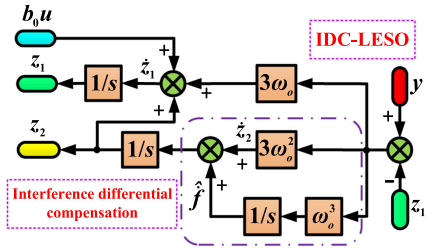

Fig. 2. Control structure diagram of IDC-LESO.

$$\begin{cases} \dot{z}_1 = z_2 - \beta_1\left(z_1 - x_1\right) + b_0 u \\ \dot{z}_2 = z_3 - \beta_2\left(z_1 - x_1\right) \\ \dot{z}_3 = -\beta_3\left(z_1 - x_1\right) \end{cases}. \tag{6}$$

From (6), it can be concluded that the introduction of the lumped interference differential $\dot{f}$ is increased the order of LESO.

The following equation can be obtained by Laplace transform on (6):

$$\begin{cases} Z_1(s) = \frac{\beta_1 s^2 + \beta_2 s + \beta_3}{s^3 + \beta_1 s^2 + \beta_2 s + \beta_3} Y(s) + \frac{b_0 s^2}{s^3 + \beta_1 s^2 + \beta_2 s + \beta_3} U(s) \\ Z_2(s) = \frac{\beta_2 s^2 + \beta_3 s}{s^3 + \beta_1 s^2 + \beta_2 s + \beta_3} Y(s) - \frac{b_0\beta_2 s + b_0\beta_3}{s^3 + \beta_1 s^2 + \beta_2 s + \beta_3} U(s) \\ Z_3(s) = \frac{\beta_3 s^2}{s^3 + \beta_1 s^2 + \beta_2 s + \beta_3} Y(s) - \frac{b_0\beta_3 s}{s^3 + \beta_1 s^2 + \beta_2 s + \beta_3} U(s) \end{cases} \tag{7}$$

where $Z_1(s)$, $Z_2(s)$, $Z_3(s)$, $Y(s)$, and $U(s)$ are Laplace transform of z_1, z_2, z_3, y, and u, respectively.

According to (7), the characteristic polynomial of IDC-LESO is shown as

$$P(s) = s^3 + \beta_1 s^2 + \beta_2 s + \beta_3. \tag{8}$$

Equation (8) is subjected to pole assignment. β_1, β_2, and β_3 of IDC-LESO are configured at ω_o as

$$s^3 + \beta_1 s^2 + \beta_2 s + \beta_3 = \left(s + \omega_o\right)^3. \tag{9}$$

From (9), $\beta_1 = 3\omega_o$, $\beta_2 = 3\omega_o^2$, and $\beta_3 = \omega_o^3$.

The control structure diagram of IDC-LESO can be obtained from (6) and (9), as shown in Fig. 2.

B. Interference Differential Compensation and Cascaded Linear Extended State Observer

From (6), the dynamic adjustment of the lumped interference z_2 is dependent on the differentiation of z_1 and the compensation of z_3. If the value of ω_o is set to be small, only x_1 can be observed by LESO. In this case, the observation error with large lumped interference will be caused. If the value of ω_o is set to a large value, the instability of the system will also be caused. To further enhance the observation accuracy of IDC-LESO for lumped interference, the observation error is reduced. z_2 is considered a known part, and the second level IDC-LESO2 is constructed to observe the remaining interference x_2-z_2, where (6) is used as the first level IDC-LESO1. The IDC-LESO2 is shown in the

following equation:

$$\begin{cases} \dot{v}_1 = v_2 + z_2 - l_1 (v_1 - x_1) + b_0 u \\ \dot{v}_2 = v_3 - l_2 (v_1 - x_1) \\ \dot{v}_3 = -l_3 (v_1 - x_1) \end{cases}. \tag{10}$$

The following equation can be obtained by performing Laplace transform on (10):

$$\begin{cases} V_1(s) = \frac{l_1 s^2 + l_2 s + l_3}{s^3 + l_1 s^2 + l_2 s + l_3} Y(s) + \frac{b_0 s^2}{s^3 + l_1 s^2 + l_2 s + l_3} U(s) \\ \quad + \frac{s^2}{s^3 + l_1 s^2 + l_2 s + l_3} Z_2(s) \\ V_2(s) = \frac{l_2 s^2 + l_3 s}{s^3 + l_1 s^2 + l_2 s + l_3} Y(s) - \frac{b_0 l_2 s + b_0 l_3}{s^3 + l_1 s^2 + l_2 s + l_3} U(s) \\ \quad - \frac{l_2 s + l_3}{s^3 + l_1 s^2 + l_2 s + l_3} Z_2(s) \\ V_3(s) = \frac{l_3 s^2}{s^3 + l_1 s^2 + l_2 s + l_3} Y(s) - \frac{b_0 l_3 s}{s^3 + l_1 s^2 + l_2 s + l_3} U(s) \\ \quad - \frac{l_3 s}{s^3 + l_1 s^2 + l_2 s + l_3} Z_2(s) \end{cases} \tag{11}$$

where $V_1(s)$, $V_2(s)$, and $V_3(s)$ are Laplace transform of v_1, v_2, and v_3, respectively.

According to the analysis method of IDC-LESO1, l_1, l_2, and l_3 of IDC-LESO2 are configured at ω_o, i.e., $l_1 = 3\omega_o$,$l_2 = 3\omega_o^2$, and $l_3 = \omega_o^3$.

C. E-LADRC Design for IPMSM

Based on the results of the above analysis, the E-LADRC controller based on IDC-C-LESO is shown in the following equation:

$$\begin{cases} \underbrace{\begin{aligned} \dot{z}_1 &= z_2 - 3\omega_o (z_1 - x_1) + b_0 u \\ \dot{z}_2 &= z_3 - 3\omega_o^2 (z_1 - x_1) \\ \dot{z}_3 &= -\omega_o^3 (z_1 - x_1) \end{aligned}}_{\text{IDC-LESO1}} \\ \underbrace{\begin{aligned} \dot{v}_1 &= v_2 + z_2 - 3\omega_o (v_1 - x_1) + b_0 u \\ \dot{v}_2 &= v_3 - 3\omega_o^2 (v_1 - x_1) \\ \dot{v}_3 &= -\omega_o^3 (v_1 - x_1) \end{aligned}}_{\text{IDC-LESO2}} \\ u = \frac{k_p (r - z_1) - (z_2 + v_2)}{b_0} \end{cases}. \tag{12}$$

According to the method of pole configuration in (3), k_p is configured at ω_c, i.e., $k_p = \omega_c$.

According to (12), the IPMSM outer loop controller based on E-LADRC is shown as

$$\begin{cases} \underbrace{\begin{aligned} \dot{\hat{\omega}}_r &= \hat{f} - 3\omega_o (\hat{\omega}_r - \omega_r) + \tfrac{1}{J} T_e \\ \dot{\hat{f}} &= \hat{\dot{f}} - 3\omega_o^2 (\hat{\omega}_r - \omega_r) \\ \hat{\dot{f}} &= -\omega_o^3 (\hat{\omega}_r - \omega_r) \end{aligned}}_{\text{IDC-LESO1}} \\ \underbrace{\begin{aligned} \dot{\hat{\omega}}_r &= \hat{\gamma} + \hat{f} - 3\omega_o (\hat{\omega}_r - \omega_r) + \tfrac{1}{J} T_e \\ \dot{\hat{\gamma}} &= \hat{\dot{\gamma}} - 3\omega_o^2 (\hat{\omega}_r - \omega_r) \\ \hat{\dot{\gamma}} &= -\omega_o^3 (\hat{\omega}_r - \omega_r) \end{aligned}}_{\text{IDC-LESO2}} \\ T_e = \frac{\omega_c (\omega_r^* - \hat{\omega}_r) - (\hat{f} + \hat{\gamma})}{\frac{1}{J}} \end{cases}. \tag{13}$$

According to (13), the IPMSM dual closed-loop control block diagram based on E-LADRC is shown in Fig. 3. The IDC-C-LESO control structure diagram is shown in Fig. 4.

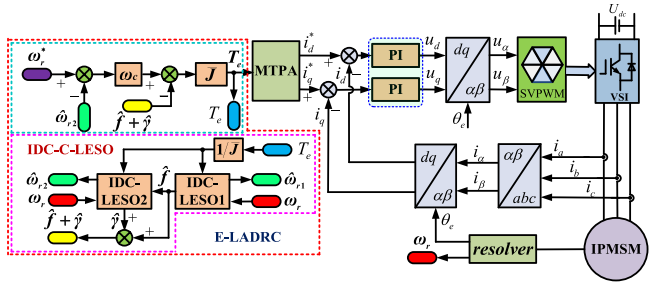

Fig. 3. IPMSM control block diagram based on E-LADRC.

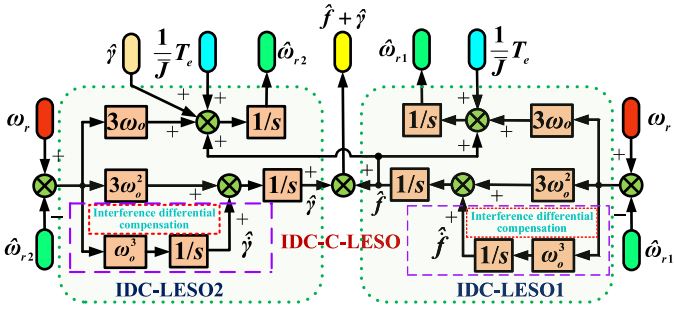

Fig. 4. IDC-C-LESO control structure diagram.

According to Figs. 3 and 4, the core of the E-LADRC proposed is still IDC-C-LESO. The known information that is easily measurable by the system is utilized by the controller: The system output (actual speed) and the system input (given speed) to observe the lumped interference experienced by the system. The lumped interference is fed back to the input of the system in the form of a state variable $f(t)$ and then compensated by the LSEF and the lumped interference link. Therefore, whether the lumped interference received by the system can be accurately compensated depends on whether the lumped interference received by the system can be accurately observed by IDC-C-LESO.

Whether IDC-C-LESO can accurately observe the key factor of lumped interference is the precise adjustment of ω_o. If ω_o is too large, it will cause system oscillation. If ω_o is too small, the interference suffered by the system (especially high-frequency interference and high-order interference) cannot be accurately observed. At present, the coupling problem between anti-interference and tracking brought by ω_o cannot be well solved by T-LESO and other improved LESO.

Therefore, the maximum purpose of the IDC-C-LESO proposed in this article is to broaden the observation range of lumped interference by LESO under the condition that ω_o is not increased. In this way, the high-frequency and high-order interferences experienced by the system can be accurately observed and compensated, and the system oscillation problem caused by excessive ω_o can be solved.

IV. Analysis of E-LADRC Control Characteristics

The stability of the system is the primary condition for its normal operation, and its dynamic characteristic and control

accuracy are marked by its anti-interference characteristic and tracking error. Therefore, the stability, interference compensation characteristic, and tracking error of the IPMSM control system based on E-LADRC are analyzed, and the parameter setting method is provided.

A. Proof of Stability

The IDC-C-LESO and the corresponding system equation of state are expressed in the form of following equations:

$$\underbrace{\begin{cases}\dot{x}_1 = x_2 + b_0 u \\ \dot{x}_2 = x_3 \\ \dot{x}_3 = \ddot{f}(x,w)\end{cases}}_{\text{state equation of the system}} \Rightarrow \underbrace{\begin{cases}\dot{z}_1 = z_2 - 3\omega_o(z_1 - x_1) + b_0 u \\ \dot{z}_2 = z_3 - 3\omega_o^2(z_1 - x_1) \\ \dot{z}_3 = -\omega_o^3(z_1 - x_1) + \ddot{f}(z,w)\end{cases}}_{\text{IDC}-\text{LESO1}} \tag{14}$$

$$\underbrace{\begin{cases}\dot{x}_1 = x_2 + z_2 + b_0 u \\ \dot{x}_2 = x_3 \\ \dot{x}_3 = \ddot{h}(x,w)\end{cases}}_{\text{state equation of the system}} \Rightarrow \underbrace{\begin{cases}\dot{v}_1 = v_2 + z_2 - 3\omega_o(v_1 - x_1) + b_0 u \\ \dot{v}_2 = v_3 - 3\omega_o^2(v_1 - x_1) \\ \dot{v}_3 = -\omega_o^3(v_1 - x_1) + \ddot{h}(v,w)\end{cases}}_{\text{IDC}-\text{LESO2}}. \tag{15}$$

Let the tracking errors of IDC-LESO1 and IDC-LESO2 be $\tilde{z}_i = x_i - z_i$ and $\tilde{v}_i = x_i - v_i$, respectively, where i = 1,2,3. The differential tracking error values of IDC-LESO1 and IDC-LESO2 can be obtained from (14) and (15), as shown in the following equation:

$$\underbrace{\begin{cases}\dot{\tilde{z}}_1 = \tilde{z}_2 - 3\omega_o\tilde{z}_1 \\ \dot{\tilde{z}}_2 = \tilde{z}_3 - 3\omega_o^2\tilde{z}_1 \\ \dot{\tilde{z}}_3 = \ddot{f}(x,w) - \ddot{f}(z,w) - \omega_o^3\tilde{z}_1\end{cases}}_{\text{IDC}-\text{LESO1}}$$

$$\underbrace{\begin{cases}\dot{\tilde{v}}_1 = \tilde{v}_2 - 3\omega_o\tilde{v}_1 \\ \dot{\tilde{v}}_2 = \tilde{v}_3 - 3\omega_o^2\tilde{v}_1 \\ \dot{\tilde{z}}_3 = \ddot{h}(x,w) - \ddot{h}(v,w) - \omega_o^3\tilde{v}_1\end{cases}}_{\text{IDC}-\text{LESO2}}. \tag{16}$$

Let $\dot{\varepsilon}_j = \tilde{z}_j/\omega_o^{j-1}$ and $\dot{\delta}_j = \tilde{v}_j/\omega_o^{j-1}$, where j = 1,2,3. Then, the following equation can be obtained:

$$\begin{pmatrix}\dot{\varepsilon} \\ \dot{\delta}\end{pmatrix} = \omega_o\begin{pmatrix}A_\varepsilon\varepsilon \\ A_\delta\delta\end{pmatrix} + \frac{1}{\omega_o^2}\begin{pmatrix}B_\varepsilon\left(\ddot{f}(x,w) - \ddot{f}(z,w)\right) \\ B_\delta\left(\ddot{h}(x,w) - \ddot{h}(v,w)\right)\end{pmatrix} \tag{17}$$

where

$$\dot{\varepsilon} = \begin{pmatrix}\dot{\varepsilon}_1 \\ \dot{\varepsilon}_2 \\ \dot{\varepsilon}_3\end{pmatrix}, \varepsilon = \begin{pmatrix}\varepsilon_1 \\ \varepsilon_2 \\ \varepsilon_3\end{pmatrix}, \dot{\delta} = \begin{pmatrix}\dot{\delta}_1 \\ \dot{\delta}_2 \\ \dot{\delta}_3\end{pmatrix}, \delta = \begin{pmatrix}\delta_1 \\ \delta_2 \\ \delta_3\end{pmatrix} \tag{18}$$

$$A_\varepsilon = A_\delta = \begin{pmatrix}-3 & 1 & 0 \\ -3 & 0 & 1 \\ -1 & 0 & 0\end{pmatrix}, B_\varepsilon = B_\delta = \begin{pmatrix}0 \\ 0 \\ 1\end{pmatrix}. \tag{19}$$

According to $|\lambda E - A| = 0$, the eigenvalues of A_ε and A_δ can be obtained as $\lambda_1 = \lambda_2 = \lambda_3 = -1$. Therefore, the system composed of A_ε and A_δ is stable. According to the Lyapunov stability criterion, the positive definite symmetric matrices P_ε and P_δ must exist so that A_ε and A_δ are satisfied with the following equation:

$$\begin{pmatrix}A_\varepsilon^T P_\varepsilon \\ A_\delta^T P_\delta\end{pmatrix} + \begin{pmatrix}P_\varepsilon A_\varepsilon \\ P_\delta A_\delta\end{pmatrix} = -\begin{pmatrix}E \\ E\end{pmatrix} \tag{20}$$

where E is the identity matrix.

From (20), the following equation can be obtained:

$$P_\varepsilon = P_\delta = \begin{pmatrix}1 & -\frac{1}{2} & -1 \\ -\frac{1}{2} & 1 & -\frac{1}{2} \\ -1 & -\frac{1}{2} & 4\end{pmatrix} \tag{21}$$

The Lyapunov function is defined as $\Gamma(\eta) = \eta^T P_\eta \eta$, and the following equation can be obtained from (17):

$$\begin{pmatrix}\dot{\Gamma}(\varepsilon) \\ \dot{\Gamma}(\delta)\end{pmatrix} = -\omega_o\begin{pmatrix}\|\varepsilon\|_2^2 \\ \|\delta\|_2^2\end{pmatrix} + \frac{2}{\omega_o^2}\begin{pmatrix}\varepsilon^T P_\varepsilon B_\varepsilon\left(\ddot{f}(x,w) - \ddot{f}(z,w)\right) \\ \delta^T P_\delta B_\delta\left(\ddot{h}(x,w) - \ddot{h}(v,w)\right)\end{pmatrix}. \tag{22}$$

Since $\ddot{f}(x,w)$, $\ddot{f}(z,w)$, $\ddot{h}(x,w)$, and $\ddot{h}(v,w)$ are satisfied by Lipschitz continuity theorem conditions in the domain of a function, then constants c_ε and c_δ greater than zero must exist so that all x, z, v, and w are satisfied by

$$\begin{cases}\left|\ddot{f}(x,w) - \ddot{f}(z,w)\right| \le c_\varepsilon\|x - z\|_2 \\ \left|\ddot{h}(x,w) - \ddot{h}(v,w)\right| \le c_\delta\|x - v\|_2\end{cases}. \tag{23}$$

By combining (22) and (23), the following equation can be obtained:

$$\begin{cases}\frac{2\varepsilon^T P_\varepsilon B_\varepsilon\left|\ddot{f}(x,w) - \ddot{f}(z,w)\right|}{\omega_o^2} \le \frac{2\varepsilon^T P_\varepsilon B_\varepsilon\|x - z\|_2}{\omega_o^2} \\ \frac{2\delta^T P_\delta B_\delta\left|\ddot{h}(x,w) - \ddot{h}(v,w)\right|}{\omega_o^2} \le \frac{2\delta^T P_\delta B_\delta\|x - v\|_2}{\omega_o^2}\end{cases}. \tag{24}$$

When $\omega_o \ge 1$, the following equation is obtained:

$$\begin{cases}\frac{\|x - z\|_2}{\omega_o^2} = \frac{\|\tilde{z}\|_2}{\omega_o^2} = \frac{\sqrt{\varepsilon_1^2 + \omega_o^2\varepsilon_2^2 + \omega_o^4\varepsilon_3^2}}{\omega_o^2} \le \|\varepsilon\|_2 \\ \frac{\|x - v\|_2}{\omega_o^2} = \frac{\|\tilde{v}\|_2}{\omega_o^2} = \frac{\sqrt{\delta_1^2 + \omega_o^2\delta_2^2 + \omega_o^4\delta_3^2}}{\omega_o^2} \le \|\delta\|_2\end{cases}. \tag{25}$$

Then, the following equation is obtained:

$$\begin{cases}\|P_\varepsilon B_\varepsilon c_\varepsilon\|_2^2 - 2\|P_\varepsilon B_\varepsilon c_\varepsilon\|_2 + 1 \ge 0 \\ \|P_\delta B_\delta c_\delta\|_2^2 - 2\|P_\delta B_\delta c_\delta\|_2 + 1 \ge 0\end{cases}. \tag{26}$$

By combining (24)–(26), the following equation can be obtained:

$$\begin{cases}\frac{2\varepsilon^T P_\varepsilon B_\varepsilon\left|\ddot{f}(x,w) - \ddot{f}(z,w)\right|}{\omega_o^2} \le \left(\|P_\varepsilon B_\varepsilon c_\varepsilon\|_2^2 + 1\right)\|\varepsilon\|_2^2 \\ \frac{2\delta^T P_\delta B_\delta\left|\ddot{h}(x,w) - \ddot{h}(v,w)\right|}{\omega_o^2} \le \left(\|P_\delta B_\delta c_\delta\|_2^2 + 1\right)\|\delta\|_2^2\end{cases}. \tag{27}$$

The following equation can be obtained from (22) and (27):

$$\begin{cases}\dot{\Gamma}(\varepsilon) \le -\omega_o\|\varepsilon\|_2^2 + (\|P_\varepsilon B_\varepsilon c_\varepsilon\| + 1)\|\varepsilon\|_2^2 \\ \dot{\Gamma}(\delta) \le -\omega_o\|\delta\|_2^2 + (\|P_\delta B_\delta c_\delta\| + 1)\|\delta\|_2^2\end{cases}. \tag{28}$$

When (29) is satisfied, the following equation is established:

$$\begin{cases} \omega_o \geq \|P_\varepsilon B_\varepsilon c_\varepsilon\|_2^2 + 1 \\ \omega_o \geq \|P_\delta B_\delta c_\delta\|_2^2 + 1 \end{cases} \tag{29}$$

$$\begin{cases} \dot{\Gamma}(\varepsilon) < 0 \\ \dot{\Gamma}(\delta) < 0 \end{cases}. \tag{30}$$

According to the Lyapunov stability criterion, the following equation is described:

$$\begin{cases} \lim\limits_{t\to\infty} \tilde{z}_i = 0 \\ \lim\limits_{t\to\infty} \tilde{v}_i = 0 \end{cases} \quad i = 1, 2, 3. \tag{31}$$

According to (31), when time approaches infinity, the estimation error of IDC-C-LESO tends to zero. Therefore, the IDC-C-LESO is converged.

Assuming that the input and output of the system are bounded, the following equation can be obtained from (12):

$$\dot{y} = f - z_2 - v_2 + \omega_c (r - z_1) + \dot{r}. \tag{32}$$

Let $\alpha = r\text{-}x_1$. The following equation can be obtained from (32):

$$\dot{\alpha} = D\alpha + Qe \tag{33}$$

where $D = (-\omega_c)$, $Q = (-\omega_c \quad -1)$, and $e = (\tilde{z}_1 \quad \tilde{z}_2 + \tilde{v}_2)^T$.

Since the IDC-C-LESO has achieved stable output, (33) is solved, and the expression of the solution is shown as

$$\delta(t) = e^{Dt}\delta(0) + \int_0^t e^{D(t-\tau)} Q e d\tau. \tag{34}$$

Due to the correlation between the stability of the system and the coefficient matrix of the system, matrix D is assigned to poles to obtain $|\lambda E - D| = \lambda + \omega_c$. Therefore, the characteristic root of D is $\lambda = -\omega_c$. According to the principle of similar diagonalization, the invertible matrix T must exist so that $D = T\text{diag}(\lambda)T^{-1}$ is established.

According to norm theory, $\|e^{Dt}\|_2 \leq \|T\|_2\|T^{-1}\|_2 e^{-\lambda t}$ can be obtained. Let $a = \|T\|_2\|T^{-1}\|_2$, then $\|e^{Dt}\|_2 \leq ae^{-\lambda t}$, i.e., $\lim\limits_{t\to\infty}\|e^{Dt}\|_2 = 0$. Similarly, when $\|e^{D(t-\tau)}\|_2 \leq ae^{-\lambda(t-\tau)}$, the following equation is established:

$$\left\|\int_0^t e^{D(t-\tau)} Q e d\tau\right\|_2 \leq \|Q\|_2 \left(\left\|\int_0^{t_0} e^{D(t-\tau)} e d\tau\right\|_2 + \left\|\int_{t_0}^t e^{D(t-\tau)} e d\tau\right\|_2\right). \tag{35}$$

Since $\lim\limits_{t\to\infty} e(t) = 0$, the 2-norm of $e(t)$ has an upper bound. If its upper bound is ρ, then $\|e\|_2 \leq \rho$. Similarly, the following equation is established:

$$\left\|\int_0^t e^{D(t-\tau)} Q e d\tau\right\|_2 \leq \frac{a\rho}{\lambda}\|Q\|_2 e^{-\lambda t}\left(1 - e^{-\lambda t}\right). \tag{36}$$

From the above analysis, it can be concluded that $\lim\limits_{t\to\infty}\frac{a\rho}{\lambda}\|Q\|_2 e^{-\lambda t}(1 - e^{-\lambda t}) = 0$, i.e., $\|\int_0^t e^{D(t-\tau)} Q e d\tau\|_2 = 0$ is established. It can be concluded that the following equation is established:

$$\lim_{t\to\infty}\alpha(t) = 0. \tag{37}$$

Based on the results of the above analysis, the closed-loop system based on E-LADRC is stable.

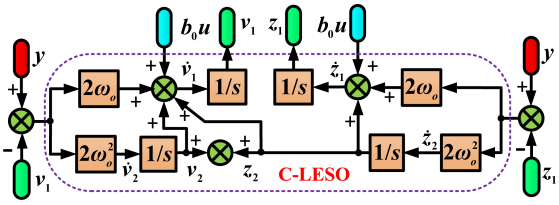

Fig. 5. Control structure diagram of C-LESO.

B. Analysis of Tracking Error

The transfer function $\Phi_{IDC-Cz_2}(s)$ of IDC-C-LESO based on the lumped interference observation value and the transfer function $\Phi_{\text{IDC-Ce}_2}(s)$ of the lumped interference observation value error can be obtained from (7) and (11), respectively, as shown in the following equations:

$$\begin{aligned} \Phi_{\text{IDC-Cz}_2} &= \frac{Z_{2\text{IDC-C}}(s) + V_{2\text{IDC-C}}(s)}{F(s)} \\ &= \frac{\left(3\omega_o^2 s + \omega_o^3\right)\left(2s^3 + 6\omega_o s^2 + 3\omega_o^2 s + \omega_o^3\right)}{\left(s^3 + 3\omega_o s^2 + 3\omega_o^2 s + \omega_o^3\right)^2} \end{aligned} \tag{38}$$

$$\begin{aligned} \Phi_{\text{IDC-Ce}_2}(s) &= \frac{F(s) - \left(Z_{2\text{IDC-C}}(s) + V_{2\text{IDC-C}}(s)\right)}{F(s)} \\ &= \frac{s^6 + 6\omega_o s^5 + 9\omega_o^2 s^4}{\left(s^3 + 3\omega_o s^2 + 3\omega_o^2 s + \omega_o^3\right)^2}. \end{aligned} \tag{39}$$

The transfer function $\Phi_{\text{IDCz}_2}(s)$ of IDC-LESO based on the lumped interference observation value and the transfer function $\Phi_{\text{IDCe}_2}(s)$ of the lumped interference observation error can be obtained from (7), as shown in the following equations:

$$\Phi_{\text{IDCz}_2}(s) = \frac{Z_{2\text{IDC}}(s)}{F(s)} = \frac{3\omega_o^2 s + \omega_o^3}{s^3 + 3\omega_o s^2 + 3\omega_o^2 s + \omega_o^3} \tag{40}$$

$$\Phi_{\text{IDCe}_2}(s) = \frac{F(s) - Z_{2\text{IDC}}(s)}{F(s)} = \frac{s^3 + 3\omega_o s^2}{s^3 + 3\omega_o s^2 + 3\omega_o^2 s + \omega_o^3}. \tag{41}$$

According to [28], the time-domain expression and control structure diagram of C-LESO can be obtained as shown in the following equation and Fig. 5, respectively:

$$\begin{cases} \underbrace{\begin{aligned} \dot{z}_1 &= z_2 - 2\omega_o(z_1 - x_1) + b_0 u \\ \dot{z}_2 &= -\omega_o^2(z_1 - x_1) \end{aligned}}_{\text{T-LESO1}} \\ \underbrace{\begin{aligned} \dot{v}_1 &= v_2 + z_2 - 2\omega_o(v_1 - x_1) + b_0 u \\ \dot{v}_2 &= -\omega_o^2(v_1 - x_1) \end{aligned}}_{\text{T-LESO2}} \end{cases}. \tag{42}$$

According to (42) and Fig. 5, the transfer function $\Phi_{Cz_2}(s)$ of C-LESO based on the lumped interference observation value and the transfer function $\Phi_{Ce_2}(s)$ of the lumped interference observation error are shown in the following equations:

$$\Phi_{Cz_2}(s)=\frac{Z_{2C}(s)+V_{2C}(s)}{F(s)}=\frac{\omega_o^2\left(2s^2+4\omega_o s+\omega_o^2\right)}{\left(s^2+2\omega_o s+\omega_o^2\right)^2} \tag{43}$$

$$\begin{aligned}\Phi_{Ce_2}(s)&=\frac{F(s)-(Z_{2C}(s)+V_{2C}(s))}{F(s)}\\&=\frac{s^2\left(s+2\omega_o\right)}{\left(s^2+2\omega_o s+\omega_o^2\right)^2}.\end{aligned} \tag{44}$$

Similarly, the transfer function $\Phi_{\mathrm{IDC-Cz_2}}(s)$ of T-LESO based on the lumped interference observation value and the transfer function $\Phi_{\mathrm{IDC-Ce_2}}(s)$ of the lumped interference observation error can be obtained from (2) and (3), respectively, as shown in the following equations:

$$\Phi_{Tz_2}(s)=\frac{Z_{2T}(s)}{F(s)}=\frac{\omega_o^2}{s^2+2\omega_o s+\omega_o^2} \tag{45}$$

$$\Phi_{Te_2}(s)=\frac{F(s)-Z_{2T}(s)}{F(s)}=\frac{s^2+2\omega_o s}{s^2+2\omega_o s+\omega_o^2}. \tag{46}$$

When the lumped interference $f(t)$ is the step interference K, slope interference Kt, and acceleration interference $Kt^2/2$, respectively (K is the interference gain coefficient). The time-domain expressions of IDC-C-LESO, IDC-LESO, C-LESO, and T-LESO based on the lumped interference tracking error can be obtained from (39), (41), (44), and (46), as shown in the following equations:

$$\begin{cases}e_{2_1\mathrm{IDC-C}}(t)=Ke^{-\omega_o t}+K\omega_o te^{-\omega_o t}-\frac{5}{2}K\omega_o^2t^2e^{-\omega_o t}\\\quad-\frac{1}{6}K\omega_o^3t^3e^{-\omega_o t}+\frac{1}{3}K\omega_o^4t^4e^{-\omega_o t}-\frac{1}{30}K\omega_o^5t^5e^{-\omega_o t}\\e_{2_2\mathrm{IDC-C}}(t)=Kte^{-\omega_o t}+K\omega_o t^2e^{-\omega_o t}-\frac{1}{2}K\omega_o^2t^3e^{-\omega_o t}\\\quad-\frac{1}{6}K\omega_o^3t^4e^{-\omega_o t}+\frac{1}{30}K\omega_o^4t^5e^{-\omega_o t}\\e_{2_3\mathrm{IDC-C}}(t)=\frac{1}{2}Kt^2e^{-\omega_o t}+\frac{1}{2}K\omega_o t^3e^{-\omega_o t}\\\quad-\frac{1}{30}K\omega_o^3t^5e^{-\omega_o t}\end{cases} \tag{47}$$

$$\begin{cases}e_{2_1\mathrm{IDC}}(t)=Ke^{-\omega_o t}+K\omega_o te^{-\omega_o t}-K\omega_o^2t^2e^{-\omega_o t}\\e_{2_2\mathrm{IDC}}(t)=Kte^{-\omega_o t}+K\omega_o t^2e^{-\omega_o t}\\e_{2_3\mathrm{IDC}}(t)=\frac{3}{\omega_o^2}-\frac{3}{\omega_o^2}Ke^{-\omega_o t}-\frac{3}{\omega_o}Kte^{-\omega_o t}-Kt^2e^{-\omega_o t}\end{cases} \tag{48}$$

$$\begin{cases}e_{2_1C}(t)=Kte^{-\omega_o t}-\frac{1}{6}K\omega_o^2t^3e^{-\omega_o t}\\e_{2_2C}(t)=\frac{1}{2}Kt^2e^{-\omega_o t}+\frac{1}{6}K\omega_o t^3e^{-\omega_o t}\\e_{2_3C}(t)=\frac{2K}{\omega_o^3}-\frac{2}{\omega_o^3}Ke^{-\omega_o t}-\frac{2}{\omega_o^2}Kte^{-\omega_o t}-\frac{1}{\omega_o}Kt^2e^{-\omega_o t}\\\quad-\frac{1}{6}K\omega_o t^3e^{-\omega_o t}\end{cases} \tag{49}$$

$$\begin{cases}e_{2_1T}(t)=Ke^{-\omega_o t}+K\omega_o te^{-\omega_o t}\\e_{2_2T}(t)=\frac{2K}{\omega_o}-\frac{2K}{\omega_o}e^{-\omega_o t}-Kte^{-\omega_o t}\\e_{2_3T}(t)=-\frac{3K}{\omega_o^2}+\frac{2K}{\omega_o}t+\frac{3K}{\omega_o^2}e^{-\omega_o t}+\frac{K}{\omega_o}te^{-\omega_o t}\end{cases} \tag{50}$$

TABLE I
OBSERVATION ERRORS OF IDC-C-LESO, IDC-LESO, C-LESO, AND T-LESO FOR DIFFERENT INTERFERENCES

$\lim_{t\to\infty} e_2(t)$	K	Kt	$Kt^2/2$
$e_{2\mathrm{ssIDC-C}}$	0	0	0
$e_{2\mathrm{ssIDC}}$	0	0	$3K/\omega_o^2$
$e_{2\mathrm{ssC}}$	0	0	$2K/\omega_o^3$
$e_{2\mathrm{ssT}}$	0	$2K/\omega_o$	∞

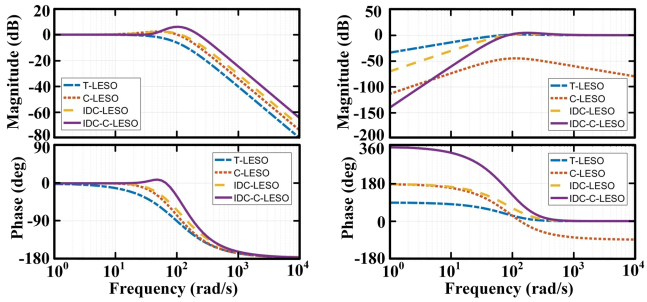

Fig. 6. Bode plots of IDC-C-LESO, IDC-LESO, C-LESO, and T-LESO based on lumped interference observation value and lumped interference observation error. (a) Bode plot of the observed lumped interference. (b) Bode plot of the lumped interference observation error.

where e_{2_1}, e_{2_2}, and e_{2_3} are the observation errors when K, Kt, and $Kt^2/2$ are affected in the system, respectively.

The observation errors of IDC-C-LESO, IDC-LESO, C-LESO, and T-LESO for different interferences can be obtained by calculating the limits of (47)–(50), as shown in Table I.

From Table I, when $f(t)$ is a step interference, the observation error of all four observers is zero. When $f(t)$ is a slope interference, there is an observation error for T-LESO, whereas the observation error for IDC-C-LESO, IDC-LESO, and C-LESO are zero. When $f(t)$ is an acceleration interference, only the observation error of IDC-C-LESO is zero. This indicates that IDC-C-LESO can eliminate observation errors caused by slope and acceleration interferences compared to IDC-LESO, C-LESO, and T-LESO.

C. Analysis of Anti-Interference and Coupling Characteristics

From (38) to (45), the transfer functions of IDC-C-LESO, IDC-LESO, C-LESO, and T-LESO based on the lumped interference observation value and the lumped interference observation error are only associated with ω_o. Therefore, when ω_o of different observers is taken as the same parameter, the Bode plots of four types of observers based on the lumped interference observation value and the lumped interference observation error can be obtained, as shown in Fig. 6.

From Fig. 6(a), when ω_o is taken as the same value, the observation scope of IDC-C-LESO for lumped interference is widened and its interference compensation capability is improved compared to IDC-LESO, C-LESO, and T-LESO. Thus, the stability of the system caused by magnifying ω_o is solved. From Fig. 6(b), in the low-frequency range, the observation

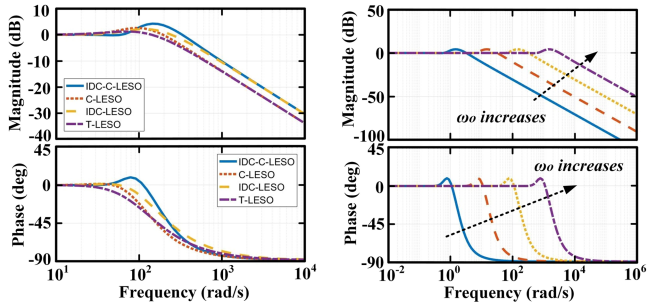

Fig. 7. Bode plots of $G(s)$ under different conditions. (a) Comparison performance analysis of four types of observes. (b) Bode plot of IDC-C-LESO as ω_o changes.

error gain of IDC-C-LESO for the lumped interference is lower than that of IDC-LESO, C-LESO, and T-LESO. Thus, the IDC-C-LESO has stronger interference compensation capability compared to IDC-LESO, C-LESO, and T-LESO and the impact of phase lag on the system has been improved.

For the tracking performance of four types of observers, the frequency domain expressions of the observed system output values for the four types of observers can be obtained from (2), (3), (7), (11), and (42), as shown in the following equation:

$$\begin{cases} V_{1\mathrm{IDC-C}}(s) = \dfrac{3\omega_o s^5+15\omega_o^2 s^4+20\omega_o^3 s^3+15\omega_o^4 s^2+6\omega_o^5 s+\omega_o^6}{(s^3+3\omega_o s^2+3\omega_o^2 s+\omega_o^3)^2} Y(s) \\ \qquad + \dfrac{b_0 s^5+3b_0\omega_o s^4}{(s^3+3\omega_o s^2+3\omega_o^2 s+\omega_o^3)^2} U(s) \\ V_{1C} = \dfrac{2\omega_o s^3+6\omega_o^2 s^2+4\omega_o^3 s+\omega_o^4}{(s^2+2\omega_o s+\omega_o^2)^2} Y(s) + \dfrac{b_0 s^3+2b_0\omega_o s^2}{(s^2+2\omega_o s+\omega_o^2)^2} U(s) \\ Z_{1\mathrm{IDC}}(s) = \dfrac{3\omega_o s^2+3\omega_o^2 s+\omega_o^3}{s^3+3\omega_o s^2+3\omega_o^2 s+\omega_o^3} Y(s) \\ \qquad + \dfrac{b_0 s^2}{s^3+3\omega_o s^2+3\omega_o^2 s+\omega_o^3} U(s) \\ Z_{1T}(s) = \dfrac{2\omega_o s+\omega_o^2}{s^2+2\omega_o s+\omega_o^2} Y(s) + \dfrac{b_0 s}{s^2+2\omega_o s+\omega_o^2} U(s) \end{cases} . \tag{51}$$

According to (51), the transfer function G(s) between the observed system output value and the actual system output value for the four types of observers is shown in as

$$\begin{cases} G_{\mathrm{IDC-C}}(s) = \dfrac{3\omega_o s^5+15\omega_o^2 s^4+20\omega_o^3 s^3+15\omega_o^4 s^2+6\omega_o^5 s+\omega_o^6}{(s^3+3\omega_o s^2+3\omega_o^2 s+\omega_o^3)^2} \\ G_C(s) = \dfrac{2\omega_o s^3+6\omega_o^2 s^2+4\omega_o^3 s+\omega_o^4}{(s^2+2\omega_o s+\omega_o^2)^2} \\ G_{\mathrm{IDC}}(s) = \dfrac{3\omega_o s^2+3\omega_o^2 s+\omega_o^3}{s^3+3\omega_o s^2+3\omega_o^2 s+\omega_o^3} \\ G_T(s) = \dfrac{2\omega_o s+\omega_o^2}{s^2+2\omega_o s+\omega_o^2} \end{cases} . \tag{52}$$

From (52), $G(s)$ of the four types of observers is only related to ω_o. Therefore, when ω_o is taken as the same value, the Bode plot of the performance comparison between the four types of observers can be obtained, as shown in Fig. 7(a). The Bode plot of IDC-C-LESO with ω_o variation is shown in Fig. 7(b).

From Fig. 7(a) and (b), under the condition that ω_o is taken as the same value, the IDC-C-LESO has a better observation ability for system output than the other three observers, and its observation ability increases with the increase of ω_o. This indicates that IDC-C-LESO has stronger tracking characteristics compared to the other three controllers.

Next, the anti-interference characteristic of E-LADRC and the coupling characteristic between its tracking ability and anti-interference ability will be further analyzed.

For E-LADRC, according to (12), the frequency domain expression of the system output including input and interference terms is expressed as

$$\begin{aligned} Y_E(s) = {} & \frac{\omega_c}{s+\omega_c} R(s) \\ & + \frac{s^6+(6\omega_o+\omega_c)s^5+(9\omega_o^2+3\omega_c\omega_o)s^4}{(s+\omega_c)\left(s^3+3\omega_o s^2+3\omega_o^2 s+\omega_o^3\right)^2} \\ & \frac{+3\omega_c\omega_o^2 s^3+\omega_c\omega_o^3 s^2}{(s+\omega_c)\left(s^3+3\omega_o s^2+3\omega_o^2 s+\omega_o^3\right)^2} F(s). \end{aligned} \tag{53}$$

For IDC-LADRC, the same LSEF and interference compensation forms as T-LADRC are adopted, as shown in (2) and Fig. 1(a). The frequency domain expression of the system output containing both input and interference terms can be obtained by combining (7), as shown in the following equation:

$$\begin{aligned} Y_{\mathrm{IDC}}(s) = {} & \frac{\omega_c}{s+\omega_c} R(s) \\ & + \frac{s^3+(3\omega_o+\omega_c)s^2}{(s+\omega_c)\left(s^3+3\omega_o s^2+3\omega_o^2 s+\omega_o^3\right)} F(s). \end{aligned} \tag{54}$$

Similarly, for C-LADRC and T-LADRC, the system output frequency domain expressions including input and interference terms can be obtained from [29], (2) and (3), which are respectively represented as

$$\begin{aligned} Y_C(s) = {} & \frac{\omega_c}{s+\omega_c} R(s) \\ & + \frac{s^4+(4\omega_o+\omega_c)s^3+(4\omega_o^2+2\omega_c\omega_o)s^2+\omega_c\omega_o^2 s}{(s+\omega_c)\left(s^2+2\omega_o s+\omega_o^2\right)^2} F(s) \end{aligned} \tag{55}$$

$$Y_T(s) = \frac{\omega_c}{s+\omega_c} R(s) + \frac{s^2+(2\omega_o+\omega_c)s}{(s+\omega_c)\left(s^2+2\omega_o s+\omega_o^2\right)} F(s). \tag{56}$$

According to (53), the closed-loop transfer function $\frac{Y_E(s)}{R(s)}$ of the system output relative to the input term and the closed-loop transfer function $\frac{Y_E(s)}{F(s)}$ of the system output relative to the interference term based on E-LADRC are shown in the following equations:

$$\frac{Y_E(s)}{R(s)} = \frac{\omega_c}{s+\omega_c} \tag{57}$$

$$\frac{Y_E(s)}{F(s)} = \frac{s^6+(6\omega_o+\omega_c)s^5+\left(9\omega_o^2+3\omega_c\omega_o\right)s^4}{(s+\omega_c)\left(s^3+3\omega_o s^2+3\omega_o^2 s+\omega_o^3\right)^2} \frac{+3\omega_c\omega_o^2 s^3+\omega_c\omega_o^3 s^2}{(s+\omega_c)\left(s^3+3\omega_o s^2+3\omega_o^2 s+\omega_o^3\right)^2}. \tag{58}$$

From (57), $\frac{Y_E(s)}{R(s)}$ of E-LADRC is only related to ω_c and has the same tracking characteristics as the other three controllers (IDC-LADRC, C-LADRC, and T-LADRC). The Bode plot of $\frac{Y_E(s)}{R(s)}$ changing with ω_c is shown in Fig. 8(a). From the figure, the tracking ability of the system for input items is enhanced with the increase of ω_c. From (58), $\frac{Y_E(s)}{F(s)}$ of E-LADRC is related to ω_c

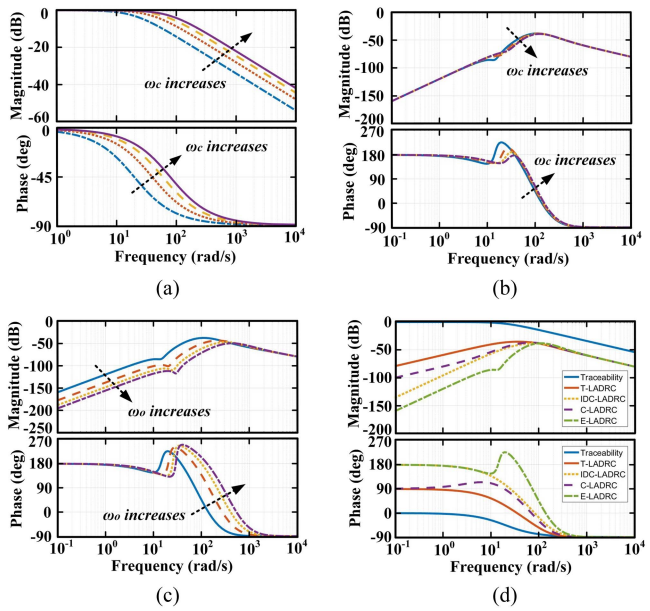

Fig. 8. Bode plots of tracking, anti-interference, and coupling characteristics of E-LADRC. (a) Bode plot for tracking characteristics. (b) Bode plot of anti-interference characteristic (only ω_c is changed). (c) Bode plot of anti-interference characteristic (only ω_o is changed). (d) Bode plot of coupling characteristic.

and ω_o. The Bode plots of $\frac{Y_E(s)}{F(s)}$ with changes in ω_c and ω_o are shown in Fig. 8(b) and (c). From the figure, the anti-interference characteristic of E-LADRC is mainly influenced by ω_o, and its anti-interference ability is enhanced with the increase of ω_o. The anti-interference ability of E-LADRC will not be significantly altered by changes in ω_c.

The Bode plot of the coupling between the tracking ability and anti-interference ability of the four controllers under the same ω_c and ω_o conditions is shown in Fig. 8(d). At the same time, combined with Fig. 7(a), under the condition that ω_o is taken as the same value, the tracking characteristic of E-LADRC is enhanced while its anti-interference characteristic is also improved. It can be concluded that the coupling problem between tracking capability and anti-interference capability can be directly solved by E-LADRC. Other controllers can only solve this problem by increasing ω_o. Thus, under the condition that ω_o is not increased, the coupling between the system tracking ability and anti-interference ability can be reduced by E-LADRC while also avoiding the problem of system oscillation caused by the increase of ω_o.

D. Parameter Setting of the Controller

The selection of LADRC order should match the order of the controlled object, i.e., the order of LADRC is equal to the order of the controlled system. From (1), the motion equation of IPMSM is a first-order differential equation, therefore the first-order LADRC is chosen as the outer loop controller of the IPMSM drive system. The reason for using a controller with the same order as the system is mainly determined by the number of state variables that need to be selected in the system. According to (5) and (13), the introduction of interference differential compensation signal into IDC-C-LESO, the order of LESO has been changed from the original second-order to the third-order, LSEF is still controlled by first-order feedforward control. Moreover, the observer feedback gain coefficient of C-LESO has been increased to six. However, according to the pole allocation method, the feedback gain coefficients of IDC-LESO1 and IDC-LESO2 are all configured as ω_o. Therefore, the ω_o values of IDC-LESO1 and IDC-LESO2 are taken as the same parameter values during parameter setting.

From (5) and (13), the parameters that need to be set include ω_o, ω_c, and b_0. Among them, $b_0 = 1/\bar{J}$ (b_0 is set as the reciprocal of the nominal value of J). But in actual engineering parameter setting, b_0 is usually maintained within the $\pm 5\%$ error range of the theoretical value, i.e., $b_0 \in [(1-5\%)\frac{1}{\bar{J}}, (1+5\%)\frac{1}{\bar{J}}]$ [30]. For the motion equation of IPMSM, it can also be expressed as

$$\dot{\omega}_r = \frac{1}{\hat{J}}T_e + \frac{J\hat{J} - J\bar{J} \pm \Delta J\hat{J}}{J\bar{J}\hat{J}}T_e \mp \frac{\Delta J}{\bar{J}}\dot{\omega}_r - \frac{1}{\bar{J}}T_L - \frac{B_r}{\bar{J}}\omega_r + d_r. \tag{59}$$

For (59), the expressions for f and b_0 are shown as

$$\begin{cases} f = \frac{J\hat{J} - J\bar{J} \pm \Delta J\hat{J}}{J\bar{J}\hat{J}}T_e \mp \frac{\Delta J}{\bar{J}}\dot{\omega}_r - \frac{1}{\bar{J}}T_L - \frac{B_r}{\bar{J}}\omega_r + d_r \\ b_0 = \frac{1}{\hat{J}} \end{cases}. \tag{60}$$

According to (60), b_0 is configured as the observed value of J and needs to be adjusted online, thereby increasing the difficulty of parameter setting. The observed value of $\hat{J}$ usually needs to be adjusted within a certain range $[J-\varepsilon, J+\varepsilon]$ (ε is a positive real number) of its actual value. According to the configuration method shown in (4), when b_0 is configured as $\bar{J}$, the difference ΔJ between it and the actual value is directly included in the range of lumped interference, and then compensated by LADRC. This not only clarifies the physical meaning of b_0 but also reduces the difficulty of parameter setting.

For most industrial control systems, ω_o and ω_c are satisfied by the relationship $\omega_o = (3\text{–}5)\omega_c$ [31]. Whether it is T-LADRC or E-LADRC, only ω_o needs to be set.

In addition, due to the delay characteristic present in most industrial control systems, ω_o needs to be smaller than $2/T_s$ (T_s is the sampling time). For (29), $\|P_\varepsilon B_\varepsilon c_\varepsilon\|_2^2 + 1 = \|P_\delta B_\delta c_\delta\|_2^2 + 1 = 5.25c^2 + 1$ (where $c_\varepsilon = c_\delta = c$) can be obtained. It can be concluded that the parameter setting scope of ω_o is $\omega_o \in [5.25c^2+1, 2/T_s)$.

V. Experimental Verification

To further prove the validity and availability of the E-LADRC proposed in this article, a 2-kW FOC experimental platform of IPMSM is built. Among them, the experimental platform is shown in Fig. 9. The program flowchart based on E-LADRC is shown in Fig. 10. The design and execution process of the proposed method is shown in Fig. 11. The nominal values of the identified motor parameters are shown in Table II.

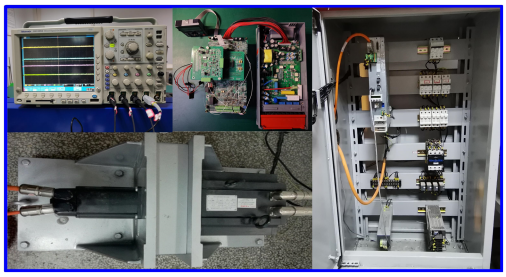

Fig. 9. FOC experimental platform of IPMSM.

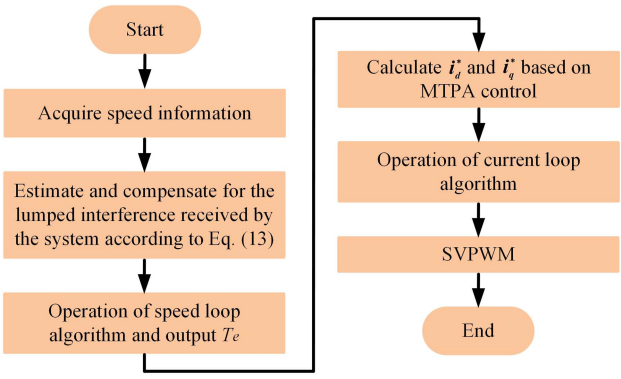

Fig. 10. Program flowchart based on E-LADRC.

TABLE II
NOMINAL VALUE OF MOTOR PARAMETERS

Parameter	Value
Rated power (kW)	2
Rated voltage (V)	380
Rated speed (r/min)	1000
d-axis inductance (H)	0.01085
q-axis inductance (H)	0.02552
Moment of inertia (kg·m^2)	0.011
Stator resistance (Ω)	1.351
Permanent magnet flux linkage (Wb)	0.77

TABLE III
CONTROLLER PARAMETERS

Parameter	ω_c (rad/s)	ω_o (rad/s)	b_0
IDC-LADRC	32	155	91
E-LADRC	47	155	91

The IDC-LADRC based on IDC-LESO and E-LADRC are compared in this section. The LSEF and interference compensation links of IDC-LADRC are designed according to (2) and (3).

To ensure that E-LADRC and IDC-LADRC are compared and analyzed under the same ω_o, according to Section IV-C and in combination with [30] and [31], ω_o in IDC-LADRC and E-LADRC will be configured with equal optimal parameter value, as shown in Table III.

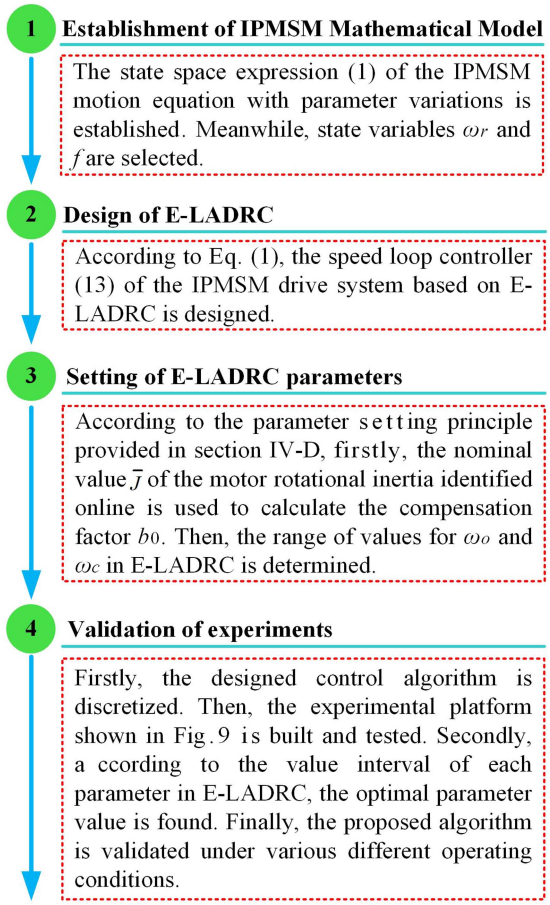

Fig. 11. Design process of the proposed method.

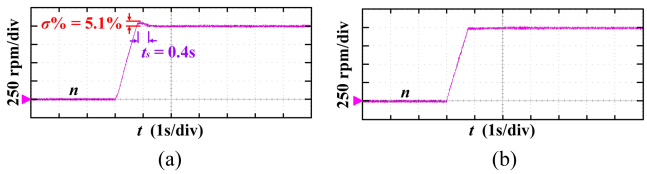

Fig. 12. Speed waveform of the motor under +1000 r/min no-load operation. (a) IDC-LADRC. (b) E-LADRC.

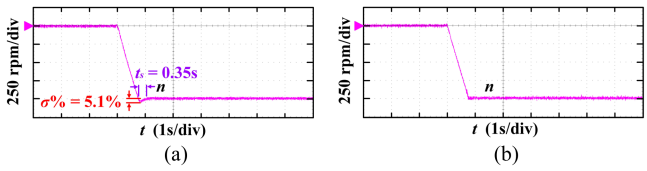

Fig. 13. n waveform of the motor under −1000 r/min no-load operation. (a) IDC-LADRC. (b) E-LADRC.

A. Verification of Traceability

The speed n waveform of the motor under no-load operation at +1000 r/min and −1000 r/min are shown in Figs. 12 and 13, respectively.

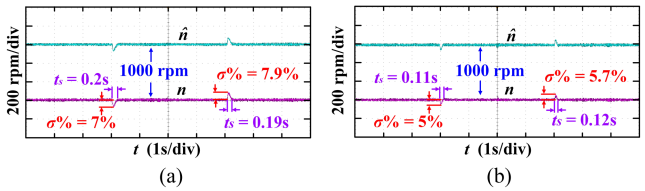

Fig. 14. $\hat{n}$ and n waveforms of the motor during loading and unloading at +1000 r/min. (a) IDC-LADRC. (b) E-LADRC.

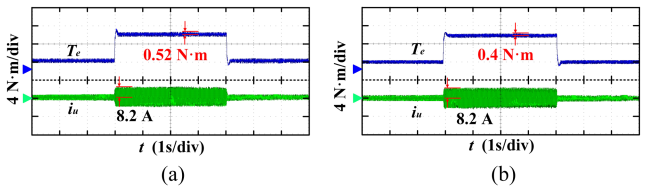

Fig. 15. T_e and U-phase current waveforms of the motor during loading and unloading at +1000 r/min. (a) IDC-LADRC. (b) E-LADRC.

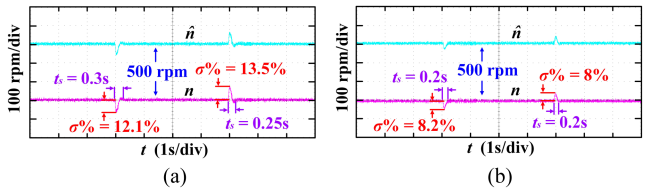

Fig. 16. $\hat{n}$ and n waveforms of the motor during loading and unloading at +500 r/min. (a) IDC-LADRC. (b) E-LADRC.

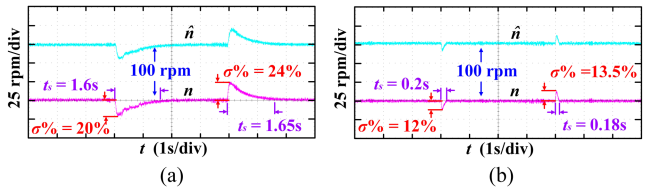

Fig. 17. $\hat{n}$ and n waveforms of the motor during loading and unloading at +100 r/min. (a) IDC-LADRC. (b) E-LADRC.

According to Fig. 12, when controlled by IDC-LADRC, the overshoot of the motor when accelerating to +1000 r/min is 5.1%, and the settling time is 0.4 s. When controlled by E-LADRC, there are no overshoot and oscillation of the speed. According to Fig. 13, when controlled by IDC-LADRC, the overshoot of the motor when accelerating to −1000 r/min is also 5.1%, and the settling time is 0.35 s. When controlled by E-LADRC, there are also no overshoot and oscillation of the speed. This indicates that E-LADRC has better tracking characteristics compared to T-LADRC.

B. Analysis of Interference Compensation Capability

To effectively verify the anti-interference characteristic of the control method proposed in this article, the loading and unloading experiments of the IPMSM drive system at different speeds will be analyzed in this section. The observed speed $\hat{n}$ and actual speed n waveforms of the motor under +1000 r/min operating conditions, as well as the output torque T_e and U-phase current waveforms, are shown in Figs. 14 and 15, respectively.

From Fig. 14, under +1000 r/min operating conditions, the speed drop of the motor controlled by IDC-LADRC is 7%, and the settling time is 0.2 s. The speed overshoot is 7.9%, and the settling time is 0.19 s. The speed drop of the motor controlled by E-LADRC is 5%, and the settling time is 0.11 s. The speed overshoot is 5.7%, and the settling time is 0.12 s. From Fig. 15, the output torque pulse controlled by IDC-LADRC is 0.52 N·m, whereas the torque pulse of the motor controlled by E-LADRC is 0.4 N·m. This indicates that E-LADRC has better interference compensation capability than IDC-LADRC at +1000 r/min.

The $\hat{n}$ and n waveforms of the motor under operating conditions of +500 r/min and +100 r/min are shown in Figs. 16 and 17, respectively. At the same time, the changes in speed drop, speed overshoot, and settling time when the motor is controlled by two different controllers under different speed operating conditions are shown in Tables IV and V, respectively.

TABLE IV
COMPARISON OF SPEED DROP AND SPEED OVERSHOOT

σ%	100 r/min		500 r/min		1000 r/min	
	load	unload	load	unload	load	unload
IDC-LADRC	20%	24%	12.1%	13.5%	7%	7.9%
E-LADRC	12%	13.5%	8.2%	8%	5%	5.7%
$\Delta\sigma$%	8%	10.5%	3.9%	5.5%	2%	2.2%

TABLE V
COMPARISON OF SPEED ADJUSTMENT TIME

t_s	100 r/min		500 r/min		1000 r/min	
	load	unload	load	unload	load	unload
IDC-LADRC	1.6s	1.65s	0.3s	0.25s	0.2s	0.19s
E-LADRC	0.2s	0.18s	0.2s	0.2s	0.11s	0.12s
Δt_s	1.4s	1.47s	0.1s	0.05s	0.09s	0.07s

According to Tables IV and V, under three different speed operating conditions of low, medium, and high speeds, the motor controlled by E-LADRC has a smaller speed drop, overshoot, and settling time compared to the situation controlled by IDC-LADRC. Especially under low-speed operating conditions, due to the increase in friction torque, the anti-interference and tracking capabilities of the motor are further reduced. Therefore, under low-speed operating conditions, the motor speed drop, overshoot, and settling time are much higher than those under medium to high-speed operation. When controlled by E-LADRC, the drop, overshoot, and settling time of the motor speed can still maintain small values. It can be concluded that E-LADRC can better solve the coupling problem between anti-interference and tracking compared to IDC-LADRC, especially under low-speed operating conditions.

To verify that E-LADRC still has good control performance under negative speed command signal. n, T_e, and U-phase current waveforms during motor loading and unloading under operating conditions of −1000 r/min are shown in Fig. 18.

From Fig. 18, under the operating conditions of -1000 r/min, the speed overshoot of the motor controlled by IDC-LADRC

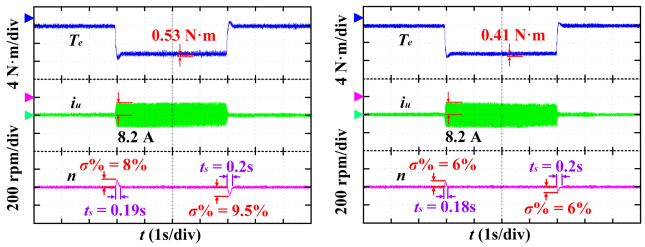

Fig. 18. n, T_e, and U-phase current waveforms of the motor during loading and unloading at −1000 r/min. (a) IDC-LADRC. (b) E-LADRC.

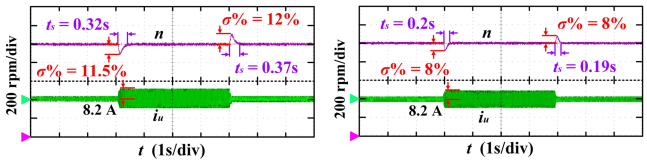

Fig. 19. n and U-phase current waveforms during loading and unloading at +1000 r/min operations (J is increased to 2J). (a) IDC-LADRC. (b) E-LADRC.

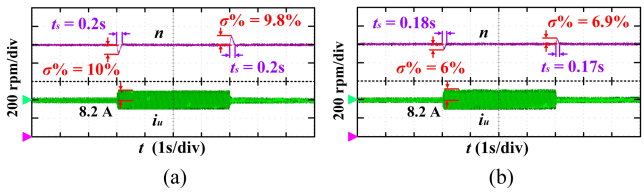

Fig. 20. n and U-phase current waveforms during loading and unloading at +1000 r/min operations (J is reduced to 0.5J). (a) IDC-LADRC. (b) E-LADRC.

is 8%, and the settling time is 0.19 s. The speed drop of the motor during unloading is 9.5%, and the settling time is 0.2 s. The torque ripple during load operation is 0.53 N·m. The speed overshoot of the motor controlled by IDC-LADRC is 6%, and the settling time is 0.18 s. The speed drop of the motor during unloading is 6%, and the settling time is 0.2 s. The torque ripple during load operation is 0.41 N·m. This indicates that even under a negative speed command signal, the E-LADRC still has better anti-interference and tracking characteristics compared to IDC-LADRC.

C. Verification of Robustness

To prove the robustness of the E-LADRC proposed to parameter changes in this article, the comparative experiment under inertial mismatch conditions is conducted in this section, where the motor is operating at +1000 r/min. The n and U-phase current waveforms when controlled by two different controllers under the conditions of increasing and reducing the J are shown in Figs. 19 and 20.

When J is mismatched, the comparative analysis results of the changes in speed and settling time are shown in Figs. 21 and 22. According to Figs. 19–22, when J is mismatched, the speed overshoot and drop of the motor under E-LADRC control

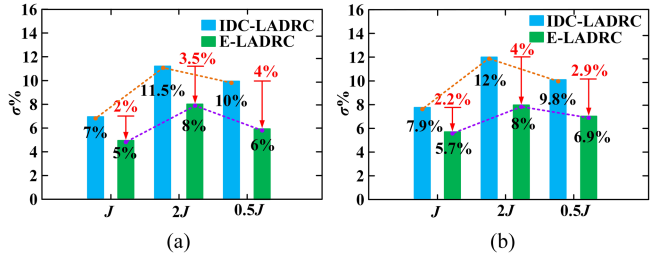

Fig. 21. Comparison results when the speed changes. (a) Load. (b) Unload.

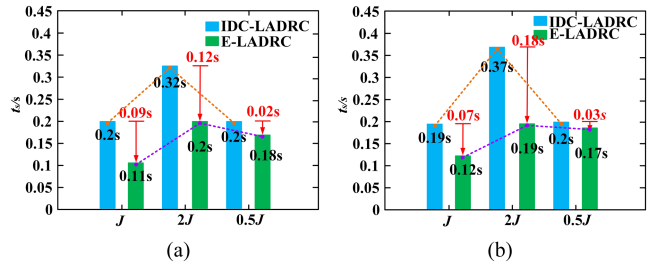

Fig. 22. Comparison results when settling time changes. (a) Load. (b) Unload.

are smaller than those under IDC-LADRC control. Similarly, when controlled by E-LADRC, the speed settling time during the loading and unloading processes is also smaller than when controlled by IDC-LADRC. In conclusion, the E-LADRC proposed in this article can suppress the control characteristic degradation caused by model mismatch compared to IDC-LADRC.

VI. Conclusion

To deal with the coupling issue between tracking and interference compensation capability of the IPMSM control system based on T-LADRC under the influence of ω_o, an E-LADRC based on IDC-C-LESO is proposed in this article. In E-LADRC, an interference differential signal is introduced, and the scope of LESO observation for lumped interference is expanded without increasing ω_o. Thus, the issue of system instability caused by oversized ω_o is avoided. The lumped interference observation error of LESO is also reduced using C-LESO. The stability, lumped interference compensation capability, and tracking error of E-LADRC are analyzed theoretically in this article, whereas the principle of controller parameter setting is given. Finally, the validity and availability of E-LADRC are verified by experiment. The analysis results indicate that the robustness and anti-interference issues caused by a moment of inertia mismatch and load interference can be solved by E-LADRC. Especially in the case of low-speed and parameter mismatch, it can solve the coupling problem between tracking and anti-interference of the system affected by ω_o, thus having a certain engineering application value. However, the method proposed in this article still has certain defects. The parameter setting scheme provided in the article can only determine ω_o within the stable scope of the system, and this scheme is not the optimal setting scheme. Next, parameter setting and optimization will be studied.

REFERENCES

[1] S. Chen, W. Ding, X. Wu, R. Hu, and S. Shi, "Finite position set-phase-locked loop with low computational burden for sensorless control of PMSM drives," *IEEE Trans. Ind. Electron.*, vol. 70, no. 9, pp. 9672–9676, Sep. 2023.

[2] J. Qu, P. Zhang, J. Jatskevich, and C. Zhang, "Torque-ripple reduction of permanent magnet synchronous machine drives based on novel speed harmonic control at low-speed operation," *IEEE Trans. Ind. Electron.*, vol. 70, no. 8, pp. 7683–7694, Aug. 2023.

[3] C. Lee and I. G. Jang, "Topology optimization framework for simultaneously determining the optimal structural design and current phase angle of the IPMSMs for the MTPA control," *IEEE Trans. Ind. Electron.*, vol. 70, no. 3, pp. 2866–2875, Mar. 2023.

[4] X. Zhang, B. Wang, Y. Yu, J. Zhang, and D. Xu, "Torque adaptive hexagon voltage extension method for PMSM flux-weakening control based on dual PI cascade structure," *IEEE Trans. Power Electron.*, vol. 38, no. 1, pp. 332–345, Jan. 2023.

[5] Y. Fan, J. Chen, Q. Zhang, and M. Cheng, "An improved inertia disturbance suppression method for PMSM based on disturbance observer and two-degree-of-freedom PI controller," *IEEE Trans. Power Electron.*, vol. 38, no. 3, pp. 3590–3599, Mar. 2023.

[6] B. Tang, W. Lu, B. Yan, K. Lu, J. Feng, and L. Guo, "A novel position speed integrated sliding mode variable structure controller for position control of PMSM," *IEEE Trans. Ind. Electron.*, vol. 69, no. 12, pp. 12621–12631, Dec. 2022.

[7] P. Zhang, Y. Chen, Z. Wan, and W. Zhang, "Adaptive finite-time backstepping sliding mode control for PMSM system with backlash," *IEEE J. Emerg. Sel. Topics Power Electron.*, vol. 10, no. 6, pp. 7549–7559, Dec. 2022.

[8] B. Li and X. Zhao, "Neural network-based adaptive sliding mode control for T-S fuzzy fractional order systems," *IEEE Trans. Circuits Syst. II, Exp. Briefs*, vol. 70, no. 12, pp. 4549–4553, Dec. 2023.

[9] W. Li, G. Feng, Z. Li, M. S. Toulabi, and N. C. Kar, "Extended Kalman filter based inductance estimation for dual three-phase permanent magnet synchronous motors under the single open-phase fault," *IEEE Trans. Energy Convers.*, vol. 37, no. 2, pp. 1134–1144, Jun. 2022.

[10] T. T. Nguyen, H. N. Tran, T. H. Nguyen, and J. W. Jeon, "Recurrent neural network-based robust adaptive model predictive speed control for PMSM with parameter mismatch," *IEEE Trans. Ind. Electron.*, vol. 70, no. 6, pp. 6219–6228, Jun. 2023.

[11] R. Sancio, S. Pugliese, K. Debbadi, M. Liserre, E. Brescia, and G. L. Cascella, "Fuzzy based adaptive linear active disturbance rejection control for a high speed PMSM," in *Proc. IEEE 1st Ind. Electron. Soc. Annu. On-Line Conf.*, 2022, pp. 1–6.

[12] X. Zhou, Y. Cui, and Y. Ma, "Fuzzy linear active disturbance rejection control of injection hybrid active power filter for medium and high voltage distribution network," *IEEE Access*, vol. 9, pp. 8421–8432, 2021.

[13] J. Han, "From PID to active disturbance rejection control," *IEEE Trans. Ind. Electron.*, vol. 56, no. 3, pp. 900–906, Mar. 2009.

[14] Z. Gao, "Scaling and bandwidth-parameterization based controller tuning," in *Proc. Amer. Control Conf.*, 2003, pp. 4989–4996.

[15] Y. Zuo, J. Chen, X. Zhu, and C. H. T. Lee, "Different active disturbance rejection controllers based on the same order GPI observer," *IEEE Trans. Ind. Electron.*, vol. 69, no. 11, pp. 10969–10983, Nov. 2022.

[16] M. Tian, B. Wang, Y. Yu, Q. Dong, and D. Xu, "Adaptive active disturbance rejection control for uncertain current ripples suppression of PMSM drives," *IEEE Trans. Ind. Electron.*, vol. 71, no. 3, pp. 2320–2331, Mar. 2024.

[17] G. Wang, R. Liu, N. Zhao, D. Ding, and D. Xu, "Enhanced linear ADRC strategy for HF pulse voltage signal injection-based sensorless IPMSM drives," *IEEE Trans. Power Electron.*, vol. 34, no. 1, pp. 514–525, Jan. 2019.

[18] L. Zhu et al., "Nonlinear active disturbance rejection control strategy for permanent magnet synchronous motor drives," *IEEE Trans. Energy Convers.*, vol. 37, no. 3, pp. 2119–2129, Sep. 2022.

[19] Q. Xu, S. Fang, P. Wan, Y. Wang, and D. Huang, "Low-speed LADRC for permanent magnet synchronous motor with high-pass speed compensator," *IEEE J. Emerg. Sel. Topics Power Electron.*, vol. 11, no. 6, pp. 6016–6027, Dec. 2023.

[20] H. Cao et al., "Improved ADRC with a cascade extended state observer based on quasi-generalized integrator for PMSM current disturbances attenuation," *IEEE Trans. Transp. Electrific.*, vol. 10, no. 1, pp. 2145–2157, Mar. 2024.

[21] L. Zhu, G. Zhang, Y. Li, G. Wang, and D. Xu, "Active disturbance rejection control for position sensorless permanent magnet synchronous motor drives based on cascade extended state observer," *Trans. China Electrotech. Soc.*, vol. 37, no. 18, pp. 4614–4624, Sep. 2022.

[22] P. Lin, S. Zhang, Z. Wu, J. Li, and X. Sun, "A linear–nonlinear switching active disturbance rejection voltage controller of PMSG," *IEEE Trans. Transp. Electrific.*, vol. 8, no. 3, pp. 3367–3378, Sep. 2022.

[23] Q. Hou, Y. Zuo, J. Sun, C. H. T. Lee, Y. Wang, and S. Ding, "Modified nonlinear active disturbance rejection control for PMSM speed regulation with frequency domain analysis," *IEEE Trans. Power Electron.*, vol. 38, no. 7, pp. 8126–8134, Jul. 2023.

[24] S. Li, J. Su, and G. Yang, "Flux weakening control strategy of permanent magnet synchronous motor based on active disturbance rejection control," *Trans. China Electrotech. Soc.*, vol. 37, no. 23, pp. 6135–6144, Dec. 2022.

[25] D. Zhang, G. Liu, H. Zhou, and W. Zhao, "Adaptive sliding mode fault-tolerant coordination control for four-wheel independently driven electric vehicles," *IEEE Trans. Ind. Electron.*, vol. 65, no. 11, pp. 9090–9100, Nov. 2018.

[26] C. Bai, Z. Yin, T. Li, Y. Zhang, D. Yuan, and P. Zhang, "Backstepping control collaborative shaft torque observer for limit cycle oscillation suppression of fully closed-loop gear transmission servo system," *IEEE Trans. Power Electron.*, vol. 39, no. 4, pp. 4513–4526, Apr. 2024.

[27] Y. Wang, L. Tao, P. Wang, X. Ma, P. Cheng, and D. Zhao, "Improved linear ADRC for hybrid energy storage microgrid output-side converter," *IEEE Trans. Ind. Electron.*, vol. 69, no. 9, pp. 9111–9120, Sep. 2022.

[28] Y. Zuo, J. Mei, C. Jiang, X. Yuan, S. Xie, and C. H. T. Lee, "Linear active disturbance rejection controllers for PMSM speed regulation system considering the speed filter," *IEEE Trans. Power Electron.*, vol. 36, no. 12, pp. 14579–14592, Dec. 2021.

[29] X. Zhou, Q. Liu, Y. Ma, W. Li, and B. Xie, "A modified LADRC-based DC-link voltage controller for photovoltaic grid-connected inverters," *Electronics*, vol. 10, no. 8, Sep. 2021, Art. no. 877.

[30] Y. Cui, Z. Yin, P. Luo, D. Yuan, and J. Liu, "Linear active disturbance rejection control of IPMSM based on quasi-proportional resonance and disturbance differential compensation linear extended state observer," *IEEE Trans. Ind. Electron.*, to be published, doi: 10.1109/TIE.2024.3352154.

[31] Y. Cui, Z. Yin, F. Gao, Y. Zhang, Y. Liu, and J. Liu, "Speed control of IPMSM based on series connection leading correction linear active disturbance rejection controller," *IEEE Trans. Power Electron.*, vol. 39, no. 3, pp. 3096–3108, Mar. 2024.

Yangyang Cui was born in Shandong, China, in 1996. He received the B.S. degree in electrical engineering and automation from the Shandong University of Aeronautics, Binzhou, China, in 2018, and the M.S. degree in electrical engineering from the Tianjin University of Technology, Tianjin, China, in 2021. He is currently working toward the Ph.D. degree in electrical engineering with Xi'an University of Technology, Xi'an, China.

His current research focuses on active disturbance rejection control of permanent magnet synchronous motors.

Zhonggang Yin (Member, IEEE) was born in Shandong, China, in 1982. He received the B.S., M.S., and Ph.D. degrees in electrical engineering from the Xi'an University of Technology, Xi'an, China, in 2003, 2006, and 2009, respectively.

Since 2009, he has been a Professor with the Department of Electrical Engineering, Xi'an University of Technology. His research interests include high-performance control of ac motors and digital control of power converters.

Xiaobo Cao was born in Shanxi, China, in 1999. He received the B.S. degree in electronic engineering in 2022 from Xi'an University of Technology, Xi'an, China, where he is currently working toward the Ph.D. degree in electrical engineering.

His current research focuses on the structural design and reliability analysis of SiC MOSFETs.

Yanqing Zhang (Member, IEEE) received the B.S., M.S., and Ph.D. degrees in electrical engineering from Xi'an University of Technology, Xi'an, China, in 2012, 2015 and 2019, respectively.

In 2019, he was with the School of Electrical Engineering, Xi'an University of Technology. His current research focuses on high-performance control of ac motors.

Yiqi Liu (Member, IEEE) received the B.S. degree in electrical engineering from Northeast Agriculture University, Harbin, China, in 2009, the M.S. degree in electrical engineering from the Tianjin University of Technology, Tianjin, China, in 2012, and the Ph.D. degree in electrical engineering from the Harbin Institute of Technology, Harbin, China, in 2016.

From 2013 to 2015, he was a visiting Ph.D. student with the Center for Ultra-Wide-Area Resilient Electric Energy Transmission Networks, University of Tennessee, Knoxville, TN, USA, with support from the China Scholarship Council. Since 2016, he has been an Associate Professor with Northeast Forestry University, Harbin, China. His research interests include power electronics for renewable energy sources, multilevel converters, high-voltage direct-current technology, dc microgrids and energy conversion, and wireless power transfer systems.